01 Oct 2019

Prediction Of Nonlinear Vertical Settlement Of A Pile Group Consisting Of New And Existing Displacement Piles In Clay Strata

Lin Li

Weibing Gong

Missouri University of Science and Technology, weibing.gong@mst.edu

Recommended Citation

L. Li and W. Gong, "Prediction Of Nonlinear Vertical Settlement Of A Pile Group Consisting Of New And Existing Displacement Piles In Clay Strata," *Soils and Foundations*, vol. 59, no. 5, pp. 1336 - 1348, Elsevier, Oct 2019.

The definitive version is available at https://doi.org/10.1016/j.sandf.2019.06.001

HOSTED BY

ELSEVIER

Available online at www.sciencedirect.com

ScienceDirect

Soils and Foundations 59 (2019) 1336–1348

SOILS AND FOUNDATIONS

www.elsevier.com/locate/sandf

Technical Paper

Prediction of nonlinear vertical settlement of a pile group consisting of new and existing displacement piles in clay strata

Lin Li [a,b], Weibing Gong [a,*]

[a] Department of Geotechnical Engineering, Tongji University, Shanghai 200092, China
[b] Department of Civil and Environmental Engineering, Louisiana State University, Baton Rouge, LA 70803, USA

Received 7 August 2018; received in revised form 3 June 2019; accepted 10 June 2019
Available online 14 August 2019

Abstract

Reusing existing displacement piles is economical, time-saving, and environment-friendly. This paper presents an analytical approach for predicting the load carrying behavior of pile groups consisting of new and existing displacement piles. The evolutions of the undrained shear strength and shear modulus of clay adjacent to the piles from installation through consolidation to long-term ageing are investigated to determine the load carrying behavior of displacement piles. The nonlinear load-settlement behavior of an individual pile is modelled by load-transfer method, where the exponential function-based load-transfer models integrating the two developed soil parameters are employed to represent the nonlinear behavior at the pile-soil interface. The pile-pile interaction in the pile group is explored based on the shear displacement method. Combining the load-transfer method and the shear displacement method, an analytical framework is proposed for predicting the load-settlement behavior of pile groups consisting of new and existing piles. The proposed framework is validated by predicting the vertical settlement of a high-rise apartment built on a pile group consisting of 74 new displacement piles and 22 existing displacement piles during construction. Good agreement is achieved between the predicted and measured results. A parametric study is performed to explore the stiffness efficiency and the load-settlement behavior of pile groups with different layouts of new and existing piles. The results indicate that the pile group with larger ratio of the number of existing piles to the number of total piles shows both stronger stiffness and a higher load carrying capacity.

Keywords: Consolidation; Ageing; Existing displacement pile; Stiffness efficiency

1. Introduction

Over the past two decades, China has undergone rapid urbanization and land for construction has become increasingly scarce. Nowadays, more and more buildings in large populated cities, like Beijing and Shanghai, need to be constructed on sites where the original buildings were demolished but many displacement piles remain. Since these displacement piles are there on-site, it is obviously wise to reuse them in the construction of new buildings. After all, reuse not only can help save construction costs but also improve the construction environment. Because new buildings tend to be higher than the demolished ones, a certain number of new displacement piles should be added into the pile foundation to ensure that the foundation can safely support the additional loads from new buildings. However, to the authors' best knowledge, no analytical exploration on the load carrying behavior of pile groups consisting of new and existing displacement piles has been reported. Indeed, the available analytical methods merely focus on the load carrying behavior of foundations only consisting of new piles (e.g. Randolph and Wroth,

Peer review under responsibility of The Japanese Geotechnical Society.
* Corresponding author.
E-mail addresses: lli1@lsu.edu (L. Li), 12weibing_gong@tongji.edu.cn (W. Gong).

https://doi.org/10.1016/j.sandf.2019.06.001

1979a; Shen et al., 1997; Hazzar et al., 2017). There is no doubt that the lack of such analytical explorations will limit the reuse of existing displacement piles.

When new displacement piles are installed into clay, the structure of the surrounding clay is significantly disturbed and the excess pore water pressure is generated, which leads to the apparent decrease in the effective stress of the clay around new piles (Carter et al., 1979; Randolph, 2003). The decrease in the effective stress reduces the strength and stiffness of the surrounding clay and hence lowers the load carrying capacity of new displacement piles. However, existing piles have existed at the construction sites for many years, often 20 years or even longer. Thus, the clay adjacent to the existing piles has experienced sufficient consolidation and ageing. Consequently, its strength and stiffness are stronger than its original values. Due to the differences in the mechanical properties of the surrounding clay, new and existing individual piles have different load bearing mechanisms, which gives rise to the different load carrying behaviors between the pile group composed of these two types of piles and the pile group consisting of new piles only.

Therefore, to properly predict the load-settlement behavior of pile groups consisting of new and existing displacement piles, this paper investigates the effects of pile installation, subsequent consolidation and soil ageing on the undrained shear strength and shear modulus of surrounding clay, which are the two key soil parameters controlling load carrying behavior of piles. The two developed soil parameters are integrated into the load-transfer models for pile shaft and end, respectively, to represent the load-settlement behaviors of new and existing individual piles. The interaction between two individual piles in the pile group is quantified with the help of the shear displacement method. The analytical framework for predicting the load-settlement behavior of pile groups consisting of new and existing piles is proposed and validated by predicting the vertical settlement of a new building constructed on a site with many existing piles. A parametric study is conducted to explore the influences of different layouts of new and existing piles on the load carrying behavior of pile groups. This study is expected to provide solid guidance and useful suggestions to help reuse existing displacement piles when constructing new buildings, instead of just removing them.

2. Effects altering mechanical properties of clay adjacent to displacement piles

2.1. Pile installation and subsequent consolidation

The installation of a displacement pile inevitably causes disturbance to the clay around the pile, especially in the vicinity of the pile-soil interface. As a result, large deformations and excess pore water pressure are developed around the pile during installation, which change the stress state and erase the in-situ stress history of surrounding clay. At present, two major theoretical methods are available for estimating the changes in the stress state of surrounding clay caused by pile installation. One is the strain path method (SPM) (Baligh, 1985), and the other is the cavity expansion method (CEM) (e.g. Carter et al., 1979; Randolph, 2003). Compared with the SPM, the CEM has the advantage that it can derive a closed-form solution to simulate the stress changes of clay during pile installation. Besides, it does not need to be paired with the finite element analyses for the subsequent consolidation process (Sheil et al., 2015). Thus, this method not only provides a feasible tool for modelling the pile installation effects, but also facilitates the analysis on subsequent consolidation. Due to the above-mentioned advantages of CEM, it is employed in this study to model the installation of displacement piles in clay.

During pile installation, a smear zone is developed around the displacement pile due to the severe installation-induced disturbance. The clay in the smear zone is at the critical state and hence the mean effective stress remains constant regardless of further possible shearing or squeezing effects caused by installation. Based on the cavity expansion solution proposed by Li et al. (2016), the mean effective stress at the critical state around an expanded cylindrical cavity, i.e., the mean effective stress around the displacement pile immediately after installation, can be given as

$$p'_{cs} = p'_0 \left(\frac{\mathrm{OCR}}{2}\right)^{\Lambda} \tag{1}$$

where p'_0 is the initial mean effective stress of the clay; OCR is the overconsolidation ratio; and $\Lambda = 1 - \kappa/\lambda$ is the plastic volumetric strain ratio. The notations κ and λ represent the slopes of the swelling line and the loading line in the e-lnp' plane, respectively.

For the clay around the existing displacement pile, its mean effective stress increases from the ultimate mean effective stress along with the dissipation of installation-induced excess pore pressure (i.e. subsequent consolidation). However, due to the stiffness discrepancy of the clay around the displacement pile, the excess pore water pressure cannot fully transfer into the increase of mean effective stress. Hence, an effective stress transfer parameter proposed by Randolph (2003) is employed to estimate the relaxation effects on the mean effective stress using the following expression

$$\Omega = \frac{3\mathrm{OCR}}{\mu(2K_0+1)}\frac{p'_0}{u_0}\ln\left[1+\frac{\mu(2K_0+1)}{3\mathrm{OCR}}\frac{u_0}{p'_0}\right] \tag{2}$$

where K_0 is the coefficient of earth pressure at rest; μ is a constant and equals 5; and u_0 is the excess pore water pressure developed immediately after pile installation, which will be given later.

Based on the principle of effective stress and considering the stress relaxation effects, the mean effective stress of the clay around an existing displacement pile during subsequent consolidation can be given as

$$p'(t) = p'_{cs} + \Omega(u_0 - u(t)) \tag{3}$$

where $u(t)$ is the excess pore water pressure at a given time during subsequent consolidation, which will also be discussed later.

To evaluate the excess pore water pressure generated by pile installation, the solution for undrained cylindrical cavity expansion proposed by Li et al. (2016), which was developed based on the K_0-anisotropic modified Cam-clay model (Sun et al. 2004) to consider both the initial anisotropy and the stress-induced anisotropy of the clay, is used to estimate the distribution of excess pore water pressure in the surrounding clay. The solution for spherical cavity expansion presented by Cao et al. (2001) is adopted to predict the excess pore water pressure developed around the pile end. The unified expression for the distributions of excess pore water pressure around pile shaft and end immediately after pile installation can be expressed as (Cao et al., 2001; Li et al., 2016)

$$u_0 = p'_0\left(\frac{m\eta^*_p}{\sqrt{3^m}} + \frac{3K_0}{1+2K_0}\right) + p'_f\left(\sqrt{3^{m-1}}\zeta\ln\left(\frac{r_y}{r_p}\right) - \frac{\zeta}{2^{2-m}\sqrt{3^{m-1}}} \pm \frac{\sqrt{4M^2-3\zeta^2}}{6} - 1\right) \tag{4}$$

where $m = 1$ denotes the cylindrical cavity expansion and $m = 2$ indicates the spherical cavity expansion; the plus sign is taken when $K_0 \le 1$ and in contrast the minus is chosen; $\eta^*_p = M^*\sqrt{\mathrm{OCR} - 1}$ is the relative stress ratio at the elastic-plastic boundary; $M^* = \sqrt{M^2 - \eta_0^2}$ is the relative stress ratio at the critical state; $M = 6\sin\varphi'/(3 - \sin\varphi')$ is the slope of the critical state line; φ' is the effective internal friction angle; $\eta_0 = |3(1 - K_0)/(2K_0 + 1)|$ is the initial stress ratio; ζ is a parameter used to simplify the expression; r_y is the radius of plastic zone formed around the pile; and r_p is the pile radius. The expressions of r_y and ζ are given as

$$\left(\frac{r_y}{r_p}\right)^{m+1} = \frac{2\sqrt{3^m}G_0}{(m+1)p'_0\eta^*_p} \tag{5}$$

$$\zeta = \frac{2\sqrt{3\left[M^2(2K_0+1)^2 - 9(1-K_0)^2\right]}}{3(2K_0+1)} \tag{6}$$

The notation G_0 in Eq. (5) represents the shear modulus of in-situ clay, defined as (Sun et al., 2004)

$$G_0 = \frac{3(1-2v')vp'_0}{2(1+v')\kappa} \tag{7}$$

where v' is the effective Poisson's ratio; $v = 1 + e$ is the specific volume; and e denotes the void ratio. Note that the shear modulus here is assumed to be isotropic, since the anisotropy of shear modulus has trivial effects on the nonlinear behavior of soil if this behavior is involved in the analysis.

The field tests (e.g. Roy et al., 1981; Abu-Farsakh et al., 2015) indicate that the excess pore water pressure mainly dissipates in the radial direction, as shown in Fig. 1. Randolph and Wroth (1979b) presented a closed-form solution for the radial consolidation of a displacement pile, which is applicable to the distribution of excess pore water pressure during consolidation. Following this solution, the distribution of excess pore water pressure can be expressed as

$$u(t) = \sum_{n=1}^{\infty} e^{-\lambda_n^2 C_h t}\left[B_{1n}J_0(\lambda_n r) + B_{2n}Y_0(\lambda_n r)\right] \tag{8}$$

where J_0 and Y_0 are zero-order Bessel functions of the first and second kinds, respectively; λ_n denotes the eigenvalues of the Bessel function; and C_h is the coefficient of consolidation for radial horizontal drainage, which is equal to

$$C_h = \frac{2k_hG_0(1-v')}{\gamma_w(1-2v')} \tag{9}$$

where k_h is the horizontal coefficient of permeability; and γ_w is the unit weight of water. The notations B_{1n} and B_{2n} in Eq. (8) are the integration constants, which can be written as

$$B_{1n} = \frac{\int_{r_p}^{R} u_0\left[J_0(\lambda_n r) - \frac{J_0(\lambda_n R)}{Y_0(\lambda_n R)}Y_0(\lambda_n r)\right] r\mathrm{d}r}{\int_{r_p}^{R}\left[J_0(\lambda_n r) - \frac{J_0(\lambda_n R)}{Y_0(\lambda_n R)}Y_0(\lambda_n r)\right]^2 r\mathrm{d}r} \tag{10}$$

$$B_{2n} = -\frac{J_0(\lambda_n R)}{Y_0(\lambda_n R)} \tag{11}$$

where R is the radial distance from the axis of displacement pile, beyond which the excess pore water pressure is negligible. The value of R can be generally taken as 5–10 times of the radius of plastic zone developed around the pile (Randolph and Wroth, 1979b).

Substituting Eqs. (4) and (8) into Eq. (3), the mean effective stress of the clay after pile installation can be readily obtained, which will be applied to quantify the changes

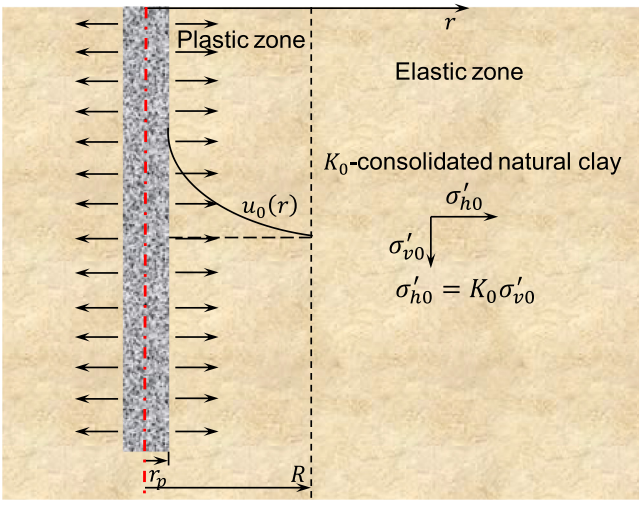

Fig. 1. Diagram of subsequent consolidation of surrounding clay.

in the undrained shear strength and shear modulus of the clay adjacent to new and existing piles in the following.

2.2. Soil ageing

Existing displacement piles tend to have been in the ground for many years. However, both the field and laboratory tests (e.g. Roy et al., 1981; Li et al., 2017a) show that the dissipation of excess pore water pressure only lasts for several months or at most several years. This indicates that the clay around existing piles not only undergoes the subsequent consolidation, but also experiences the soil ageing. In general, the soil ageing also occurs during subsequent consolidation, but the effect of ageing is very limited in the process (Augustesen, 2006). Therefore, it is assumed that the soil ageing only occurs after subsequent consolidation.

As shown in Fig. 2, the pile loading results in the increase of mean effective stress and the decrease of void ratio, which can be regarded as that the preconsolidation pressure increases from the p_0' at the point A to p_B' at the point B. During soil ageing, although the mean effective stress remains constant, the void ratio still decreases from the point B to the point C, which is equivalent to an increase in the preconsolidation pressure from p_B' to p_1'. The decreases in the void ratio leads to a more stable structure and a higher preconsolidation pressure of the clay around displacement piles. The increase in the preconsolidation pressure caused by the decrease in the void ratio is equivalent to the increase in the quasi-preconsolidation pressure, $\overline{p}_c'$ (Bjerrum, 1967; Augustesen, 2006). Here, Bjerrum's theory of time-dependent compression, i.e. the decreases in void ratio of surrounding clay induced by pile loading and soil ageing, is modeled based on the approach proposed by Garlanger (1972) as

$$e(t) = e_0 - C_c \log\left(\frac{p_L'}{p'(t_{re})}\right) - C_s \log\left(\frac{t}{t_{re}}\right), \quad t > t_{re} \tag{12}$$

where e_0 is the initial void ratio; C_c is the slope of compression curve in the e-logp' plane; p_L' is the mean effective stress of surrounding clay when the existing pile is subjected to the loads from superstructures; t_{re} is the reference time, which is assumed as the end time of dissipation of excess pore water pressure; $p'(t_{re})$ is the mean effective stress of surrounding clay corresponding to the reference time; and C_s is the secondary compression index.

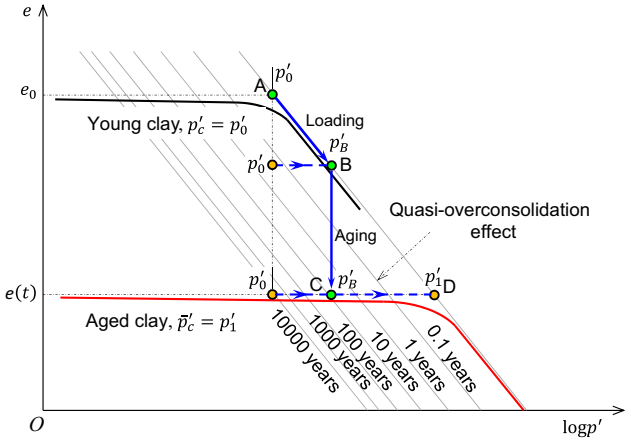

Fig. 2. Quasi-overconsolidation effect of surrounding clay.

In the $e - \ln p'$ plane, the decrease of void ratio can also be obtained as

$$\Delta e = e - e_0 = -\lambda \ln \frac{\overline{p}_c'}{p'(t_{re})} \tag{13}$$

Combining Eqs. (12) and (13) yields the quasi-preconsolidation pressure at a given time during soil ageing as

$$\frac{\overline{p}_c'}{p'(t_{re})} = \exp\left\{\frac{1}{\lambda}\left[C_c \log\left(\frac{p_L'}{p'(t_{re})}\right) + C_s \log\left(\frac{t}{t_{re}}\right)\right]\right\}, \quad t > t_{re} \tag{14}$$

To quantify the quasi-overconsolidated effects of surrounding clay, a parameter, which is referred to as the quasi-overconsolidation ratio, R_Q, can be defined as

$$R_Q(t) = \exp\left\{\frac{1}{\lambda}\left[C_c \log\left(\frac{p_L'}{p'(t_{re})}\right) + C_s \log\left(\frac{t}{t_{re}}\right)\right]\right\}, \quad t > t_{re} \tag{15}$$

3. Mechanical properties of the clay adjacent to new and existing displacement piles

Based on the concept of modified Cam-clay model, the undrained shear strength of in-situ clay can be defined as (Wood, 1990)

$$s_{u0} = \frac{1}{2} M p_0' \left(\frac{\mathrm{OCR}}{2}\right)^{\Lambda} \tag{16}$$

Pile installation not only changes the stress states of surrounding clay, but also erases the in-situ stress history of the surrounding clay, which is referred to as the remolding effect. Due to this remolding effect, the OCR of surrounding clay after installation can be taken as unity and the surrounding clay behaves like the normally consolidated clay (Randolph and Wroth, 1981). Therefore, the undrained shear strength of clay around the new displacement pile can be determined as

$$s_{u,\mathrm{new}} = \frac{1}{2} M p'(t) \left(\frac{1}{2}\right)^{\Lambda} \tag{17}$$

Apart from the pile installation and subsequent consolidation, the clay around the existing displacement pile also experiences soil ageing. As a result, the undrained shear strength and the shear modulus of clay around the existing piles are different from those around the new piles. Considering the above-mentioned effects, the undrained shear strength of clay around the existing piles can be expressed by substituting Eqs. (3) and (15) into Eq. (16) as follows

$$s_{u,\mathrm{ex}} = \frac{1}{2} M R_Q(t_a)\left[p'_{cs} + \Omega(u_0 - u(t_{re}))\right]\left(\frac{1}{2}\right)^{\Lambda}, \quad t_a > t_{re} \tag{18}$$

The clay around new displacement piles only undergoes the pile installation and subsequent consolidation. Hence, replacing p'_0 with $p'(t)$ in Eq. (7), the shear modulus of clay around new piles can be expressed as

$$G_{s,\mathrm{new}} = \frac{3(1-2v')(1+e_0)p'(t)}{2(1+v')\kappa} \tag{19}$$

Substituting Eqs. (3) and (15) into Eq. (7), the shear modulus of clay around existing piles can be given as

$$G_{s,\mathrm{ex}} = \frac{3(1-2v')\left[1+e_0 - C_c\log\left(\frac{p'_0}{p'(t_{re})}\right) - C_s\log\left(\frac{t_a}{t_{re}}\right)\right]R_Q(t_a)p'(t_{re})}{2(1+v')\kappa}, \quad t > t_{re} \tag{20}$$

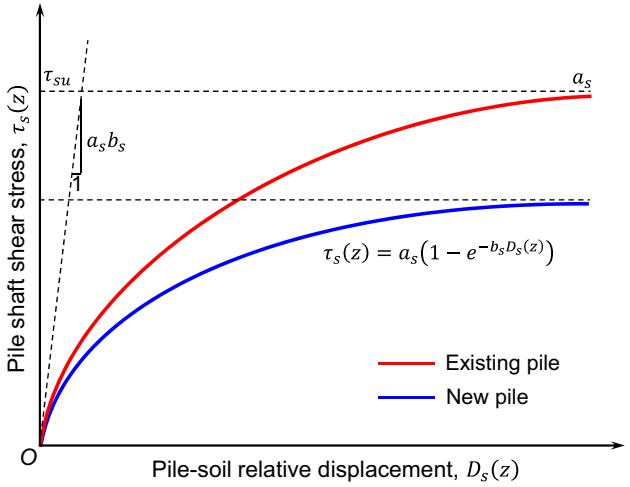

Fig. 3. Exponential load-transfer function for pile shaft.

4. Load-transfer functions

4.1. Load-transfer function for pile shaft

The load-transfer method considers the interaction between pile and surrounding soil through assuming a series of independent springs distributed along the pile shaft and at the pile end. The key of this method is to develop a rational load-transfer curve to simulate the pile-soil interaction, which has been extensively investigated in the recent decades (e.g., Wang et al., 2012; Zhang and Zhang, 2012). The results from both field and laboratory tests indicate that the relationship between the shaft shear stress, $\tau_s(z)$, and the corresponding pile-soil relative displacement, $D_s(z)$, can be reasonably described by an exponential function, which is shown in Fig. 3 and has the following expression (Wang et al., 2012)

$$\tau_s(z) = a_s\left[1 - e^{-b_s D_s(z)}\right] \tag{21}$$

where a_s and b_s are the coefficients of pile shaft load-transfer function, whose values can be easily determined based on their mechanical meanings.

It is easily found from Fig. 3 that the coefficient, a_s, represents the asymptote of load-transfer curve for the pile shaft when the pile-soil relative displacement reaches a quite large value. Hence, the coefficient, a_s, is related to the ultimate pile shaft resistance, τ_s^u, as follows

$$\tau_s^u = \lim_{D_s(z)\to\infty} \tau_s(z) = a_s \tag{22}$$

Fig. 4 illustrates the stress state of a soil element adjacent to the pile shaft during loading and the corresponding failure stress state on a Mohr's stress circle, the radius of which defines the undrained shear strength under the plane strain condition, s_u^p. It can be seen that the failure envelop is tangential to the stress circle at the point A and the stress state of the soil element at the pile-soil interface is located at the point B, as the radial effective stress becomes the largest component among the three normal stresses after pile installation (Randolph and Wroth, 1981). From the simple geometric relationship in Fig. 4, the ultimate pile shaft resistance is related to the undrained shear strength under the plane strain condition as

$$\tau_s^u = s_u^p \cos\varphi' \tag{23}$$

Note that the undrained shear strengths of the surrounding clay expressed by Eqs. (17) and (18) are developed from conventional triaxial compression tests, which is different from the undrained shear strength under the plane strain condition due to the intrinsic three-dimensional mechanical properties of the soil. Hence, the spatially mobilized plane criterion and the stress transformed method proposed by Matsuoka et al. (1999) are adopted to transform the undrained shear strength under the triaxial compression to the undrained shear strength under the plane strain condition in the following

$$s_u^p = \frac{3\sin\psi_f}{M\sqrt{2+\sin\psi_f}} s_u \tag{24}$$

where ψ_f is the stress transformed parameters, given by

$$\sin\psi_f = \frac{\sqrt{2}M}{\sqrt{9+3M}} \tag{25}$$

Substituting Eq. (24) into Eq. (23) gives the final form of the function coefficient, a_s, as

$$a_s = \frac{3\sin\psi_f\cos\varphi'}{M\sqrt{2+\sin^2\psi_f}} s_u \tag{26}$$

Taking the derivative of Eq. (21) with respect to $D_s(z)$, the tangential stiffness of pile shaft can be given as

$$K_s(z) = C_p\frac{\mathrm{d}\tau_s(z)}{\mathrm{d}D_s(z)} = 2\pi r_p a_s b_s e^{-b_s D_s(z)} \tag{27}$$

where C_p is the pile perimeter.

The elastic displacement of surrounding clay, $D_e(z)$, induced by the shaft shear stress, can be obtained based

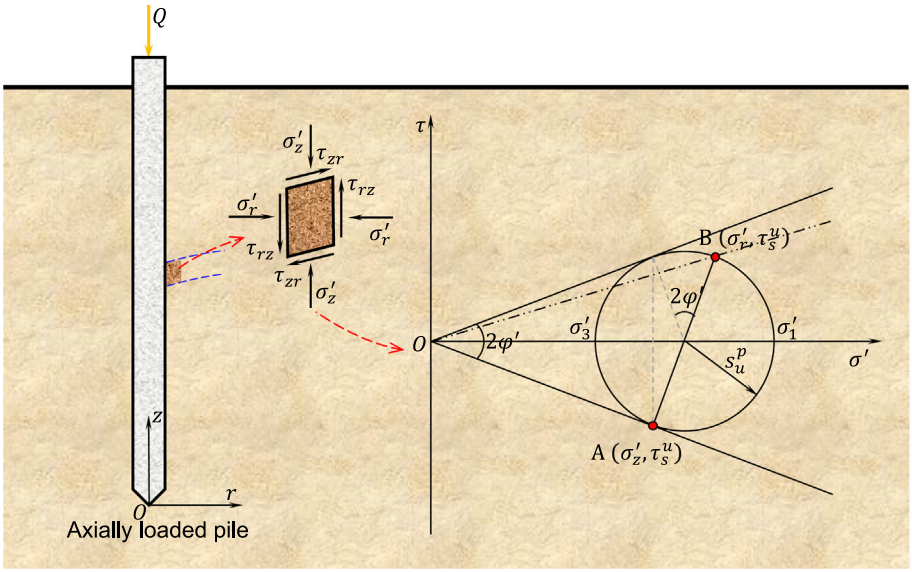

Fig. 4. Stress states of a soil element adjacent to pile shaft during pile loading and in the σ'-τ plane.

on the solution proposed by Randolph and Wroth (1979a) as

$$D_e(z) = \frac{\tau_s(z) r_p}{G_s} \ln\left(\frac{r_m}{r_p}\right) \tag{28}$$

where $r_m = 2.5L(1-v)$ is the radial distance from the pile axis, beyond which the induced shear stress is negligible. Then, the circumferential stiffness of clay, K_s^e, can be obtained as

$$K_s^e = \frac{C_p \tau_s(z)}{D_e(z)} = \frac{2\pi G_s}{\ln(r_m/r_p)} \tag{29}$$

During the initial stage of pile loading, the initial tangential stiffness of pile shaft is equal to the circumferential stiffness of clay. Hence, the circumferential stiffness, K_s^e, can be determined from Eq. (27) by taking $D_s(z)$ as zero, i.e.,

$$K_s^e = K_s|_{D_s(z)=0} = 2\pi r_p a_s b_s \tag{30}$$

Combining Eqs. (29) and (30), the coefficient, b_s, can be determined as

$$b_s = \frac{G_s}{r_p a_s \ln(r_m/r_p)} \tag{31}$$

4.2. Load-transfer function for pile end

Assuming that the load-displacement behavior developed at the pile end also obeys the exponential function, the pile end resistance, q_b, developed during pile loading can be given by

$$q_b = a_b\left(1 - e^{-b_b D_b}\right) \tag{32}$$

where D_b is the pile end displacement; and a_b and b_b are the function coefficients, whose values will be also determined based on their mechanical meanings.

Taking the derivative of Eq. (32) with respect to D_b, the tangential stiffness of pile base can be determined as

$$K_b = A_p \frac{\mathrm{d}q_b}{\mathrm{d}D_b} = \pi r_p^2 a_b b_b e^{-b_b D_b} \tag{33}$$

where A_p is the cross-sectional area of displacement pile. The function coefficient, a_b, represents the asymptote of load-transfer curve for the pile end and equals the ultimate pile base resistance, i.e.,

$$a_b = \lim_{D_b \to \infty} q_b = q_{bu} \tag{34}$$

where q_{bu} is the ultimate pile end resistance.

For a displacement pile in clay, the pile end makes much less contribution to the total pile load carrying capacity, compared with the load carrying capacity provided by pile shaft. Therefore, it is effective to simply estimate the ultimate pile end resistance via the following equation

$$q_{bu} = N_c s_u \tag{35}$$

where N_c can be empirically taken as 9 (Skempton, 1959).

The elastic stiffness of pile end can be determined by a rigid circular disc acting on the surface of a homogeneous elastic stratum, the solution of which has been provided by Randolph and Wroth (1979a) as

$$K_b^e = \frac{4 G_b r_p}{1 - v'} \tag{36}$$

From Eq. (36), the initial elastic stiffness of pile end can be expressed as

$$K_b^e = K_b|_{D_b=0} = \pi r_p^2 a_b b_b \tag{37}$$

Combining Eqs. (36) and (37) yields the function coefficient, b_b, as

$$b_b = \frac{4G_b}{\pi r_p a_b (1 - v')} = \frac{4G_b}{\pi N_c r_p (1 - v') s_u} \tag{38}$$

Substituting the undrained shear strengths and the shear moduli of clays around new and existing piles into Eqs. (26), (31), (34) and (38), the corresponding load-transfer functions for new and existing piles can be readily obtained, respectively.

5. Load-displacement behavior of a single displacement pile

The total displacement of the pile shaft, $D_{pile}(z)$, primarily consists of the nonlinear displacement developed in the shear band adjacent to the pile-soil interface, $D_s(z)$, as well as the purely elastic displacement outside the shear band, $D_e(z)$ (see Fig. 5), i.e.,

$$D_{soil}(z) = D_s(z) + D_e(z) \tag{39}$$

where the elastic displacement has been given by Eq. (28) and can be rewritten as

$$D_e(z) = \chi\tau_s(z) \tag{40}$$

where $\chi = (r_p/G_s)\ln(r_m/r_p)$.

On the other hand, the displacement at the top of pile segment is composed of the compression of pile shaft and the displacement of pile end, i.e.

$$D_p(z) = \int_0^z \frac{Q(z)}{E_pA_p}\mathrm{d}z + D_b \tag{41}$$

where E_p is the elastic modulus of displacement pile; $Q(z)$ is the load applied to the pile segment head; and D_b is the settlement of pile end.

From Eqs. (40) and (41), the nonlinear displacement developed in the shear band adjacent to the pile soil interface, $D_s(z)$, can be calculated as

$$D_s(z) = D_p(z) - D_e(z) = \int_0^z \frac{Q(z)}{E_pA_p}\mathrm{d}z + D_b - \chi\tau_s(z) \tag{42}$$

Making use of Eq. (42), the force provided by the pile shaft resistance, $F(z)$, can be written as

$$F(z) = K_s\int_0^z D_s(z)\mathrm{d}z = K_s\int_0^z\left[\int_0^z \frac{Q(z)}{E_pA_p}\mathrm{d}z + D_b - \chi\tau_s(z)\right]\mathrm{d}z \tag{43}$$

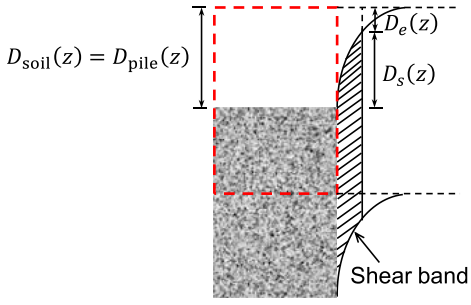

Fig. 5. Displacements of pile segment and surrounding clay.

The axial load of the pile at depth, z, are the sum of the shaft and end forces. With the aid of Eq. (43), the axial load $Q(z)$ can be given as

$$Q(z) = K_bD_b + F(z) = K_bD_b + K_sD_bz + K_s\int_0^z\left[\int_0^z \frac{Q(z)}{E_pA_p}\mathrm{d}z - \chi\tau_s(z)\right]\mathrm{d}z \tag{44}$$

The mechanical meaning of the derivative of axial load with respect to depth, z, gives

$$Q'(z) = \frac{\mathrm{d}Q(z)}{\mathrm{d}z} = 2\pi r_p\tau_s(z) \tag{45}$$

Combining Eqs. (44) and (45), along with assuming $\xi = \chi/(2\pi r_p)$ and $y = \int_0^z Q(z)\mathrm{d}z$, yields

$$(1+\xi K_s)y'' - \frac{K_s}{E_pA_p}y - K_sD_b = 0 \tag{46}$$

It can be found that the above equation is a second-order differential equation, the solution of which can be obtained as

$$y(z) = \int_0^z Q(z)\mathrm{d}z = \left(c_1e^{rz} + c_2e^{-rz} - E_pA_p\right)D_b \tag{47}$$

Based on the coordinates system defined in Fig. 4, the boundary conditions of Eq. (47) can be expressed as $y(0) = 0$ and $y'(0) = K_bD_b$. Substituting the boundary conditions into the equation, the values of r, c_1 and c_2 can be calculated as

$$r = \sqrt{\frac{K_s}{(1+\xi K_s)E_pA_p}} \tag{48}$$

$$c_1 = \frac{K_b + E_pA_pr}{2r} \tag{49}$$

$$c_2 = \frac{-K_b + E_pA_pr}{2r} \tag{50}$$

Substituting Eqs. (48)–(50) back into Eq. (47), the displacements of pile end and head can be obtained, respectively, as

$$D_b = \frac{Q(L)}{r(c_1e^{rL} - c_2e^{-rL})} \tag{51}$$

$$D_T = \frac{Q(L)}{E_pA_pr}\frac{c_1e^{rL} + c_2e^{-rL}}{c_1e^{rL} - c_2e^{-rL}} \tag{52}$$

Taking the derivative of Eq. (47), along with the substitution of Eq. (51), yields the axial load at a given depth, z, as

$$Q(z) = \frac{Q(L)(c_1e^{rz} - c_2e^{-rz})}{c_1e^{rL} - c_2e^{-rL}} \tag{53}$$

Recalling Eq. (40) and making use of Eq. (53), the elastic displacement outside the shear band, $D_e(z)$, can be further expressed as

$$D_e(z) = \chi\tau_s(z) = \xi Q'(z) = \frac{\xi Q(L)r(c_1e^{rz} - c_2e^{-rz})}{c_1e^{rL} - c_2e^{-rL}} \tag{54}$$

The nonlinear displacement developed at the pile-soil interface and in the shear band, $D_s(z)$, can be obtained based on its mechanical meaning as

$$D_s(z) = \frac{f'(z)}{K_s} = \frac{Q'(z)}{Ks} = \frac{Q(L)r}{K_s}\frac{c_1e^{rz} + c_2e^{-rz}}{c_1e^{rL} - c_2e^{-rL}} \tag{55}$$

Also, the total displacement at the top of the pile segment can be obtained by substituting Eqs. (47) and (51) into Eq. (41) as follows

$$D_p(z) = \frac{Q(L)(c_1e^{rz} + c_2e^{-rz})}{E_pA_pr(c_1e^{rL} - c_2e^{-rL})} \tag{56}$$

In actual conditions, the soils are generally layered and thus this property should be taken into consideration when exploring the load-settlement behavior of new and existing displacement piles in clay. As shown in Fig. 6, the pile is separated into n segments based on the actual layers of clays. Based on Eqs. (52) and (53), the displacement and the axial load at the top of pile segment k can be expressed, respectively, as

$$D_k^{\text{top}} = \frac{Q(L)\left(c_{1,k}e^{r_kl(k-1)} + c_{2,k}e^{-r_kl(k-1)}\right)}{E_pA_pr_k\left(c_{1,i}e^{r_kL} - c_{2,k}e^{-r_kL}\right)} \tag{57}$$

$$Q_k^{\text{top}} = \frac{Q(L)\left(c_{1,k}e^{r_kl(k-1)} - c_{2,k}e^{-r_kl(k-1)}\right)}{c_{1,k}e^{r_kL} - c_{2,k}e^{-r_kL}} \tag{58}$$

where $l(k-1)$ is the depth of $(k-1)$th pile segment; and the expressions of r_k, $c_{1,k}$ and $c_{2,k}$ are as follows

$$r_k = \sqrt{\frac{K_{sk}}{(1+\xi K_{sk})E_pA_p}} \tag{59}$$

$$c_{1,k} = \frac{K_{bk} + E_pA_pr_k}{2r_k} \tag{60}$$

$$c_{2,k} = \frac{-K_{bk} + E_pA_pr_k}{2r_k} \tag{61}$$

With Eqs. (57) and (58), the stiffness at the top of pile segment k can be determined from its definition as

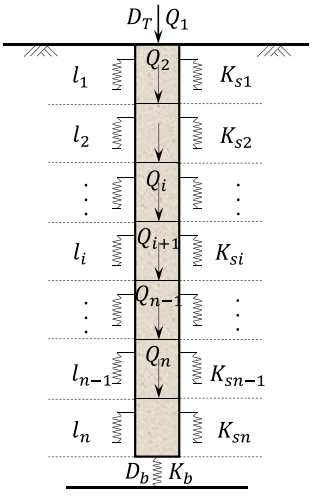

Fig. 6. Discretization of a displacement pile in layered clays.

$$K_{k-1}^{\text{end}} = \frac{Q_k^{\text{top}}}{D_k^{\text{top}}} = \frac{E_pA_pr_k\left(c_{1,k}e^{r_kl(k-1)} - c_{2,k}e^{-r_kl(k-1)}\right)}{\left(c_{1,k}e^{r_kl(k-1)} + c_{2,k}e^{-r_nl(k-1)}\right)} \tag{62}$$

6. Analysis for a pile group consisting of new and existing displacement piles

The nonlinear behavior of the pile-soil interaction primarily is displayed in the shear band adjacent to the pile-soil interface, while the soil outside the shear band generally shows the elastic behavior. Thus, it can be assumed that the displacement of adjacent pile caused by the loaded pile obeys the elastic superposition principle. As shown in Fig. 7, the total displacement of a new displacement pile, D_i^s, is composed of the nonlinear displacement, D_i^{non}, and the elastic displacement, D_{ii}^{e}, caused by its own load, the additional elastic displacement induced by the load applied on its adjacent existing pile, $D_{j,i}^{\text{e}}$, as well as the displacement reduction due to the reinforcement effect of the adjacent pile, $\widehat{D}_{j,i}^{\text{e}}$, i.e.

$$D_i^s = D_i^{\text{non}} + D_{ii}^{\text{e}} + D_{j,i}^{\text{e}} - \widehat{D}_{j,i}^{\text{e}} \tag{63}$$

The nonlinear displacement of new pile, which is caused by its own load, can be calculated from Eq. (55) as

$$D_i^{\text{non}} = \frac{Q(L)r_i}{K_{si}}\frac{c_{1,i}e^{r_il_i} + c_2e^{-r_il_i}}{c_{1,i}e^{r_iL} - c_{2,i}e^{-r_iL}} \tag{64}$$

Both the elastic displacement of new pile caused by its own load, D_{ii}^{e}, and the additional elastic displacement caused by its adjacent existing pile, $D_{j,i}^{\text{e}}$, can be calculated based on the solution proposed by Randolph and Wroth (1979a) as

$$D_{ii}^{\text{e}} = \frac{\tau_{si}r_p}{G_{si}}\ln\left(\frac{r_m}{r_p}\right) \tag{65}$$

$$D_{j,i}^{\text{e}} = \frac{\tau_{sj}r_p}{G_{sj}}\ln\left(\frac{r_m}{r_{j,i}}\right) \tag{66}$$

where τ_s is the shear stress of clay around pile shaft; and $r_{j,i}$ is the distance between the axes of new and existing piles.

For a pile group consisting of n piles, the total elastic displacement of the new pile can be obtained based on Eqs. (65) and (66) as

$$D_i^{\text{e}} = D_{ii}^{\text{e}} + D_{j,i}^{\text{e}} = \frac{\tau_{si}r_p}{G_{si}}\ln\left(\frac{r_m}{r_p}\right) + \sum_{j=1,j\neq i}^{n}\frac{\tau_{sj}r_p}{G_{sj}}\ln\left(\frac{r_m}{r_{j,i}}\right) \tag{67}$$

Because of the reinforcement effect of the adjacent piles, an elastic reaction force $\tau_{sj,i}$, of existing pile j will reduce the displacement of new pile i. Based on the transfer mechanism of shear stress, the elastic reaction force can be expressed as (Zhang and Zhang, 2012)

$$\tau_{sj,i} = \frac{r_p}{r_{j,i}}\tau_{si} \tag{68}$$

Making use of Eq. (68), the displacement reduction, $\widehat{D}_{j,i}^{\text{e}}$, resulting from the elastic reaction force can be given as

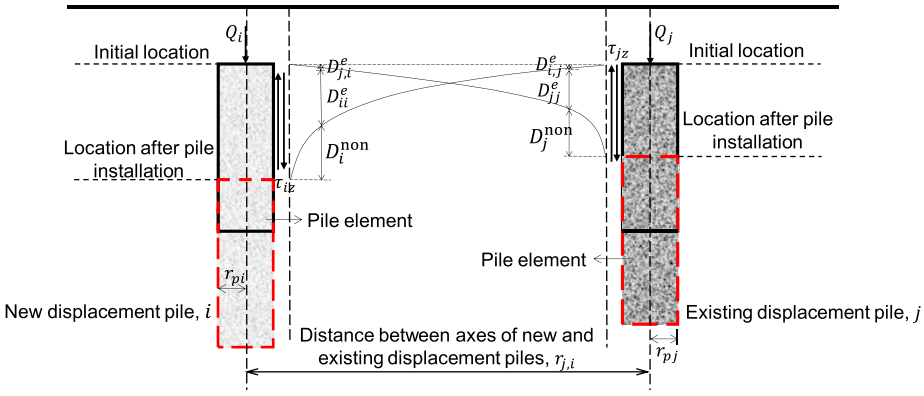

Fig. 7. Interactions between new and existing displacement piles.

$$\widehat{D}^{\mathrm{e}}_{j,i} = \frac{\tau_{sj,i} r_p}{G_{sj}} \ln\left(\frac{r_m}{r_{j,i}}\right) = \frac{\tau_{si} r_p^2}{G_{sj} r_{j,i}} \ln\left(\frac{r_m}{r_{j,i}}\right) \tag{69}$$

The total displacement reduction caused by elastic reaction force from adjacent piles in a pile group consisting of n piles can be expressed as

$$\widehat{D}^{\mathrm{e}}_{j,i} = \sum_{j=1, j\neq i}^{n} \frac{\tau_{si} r_p^2}{G_{sj} r_{j,i}} \ln\left(\frac{r_m}{r_{j,i}}\right) \tag{70}$$

The pile end displacement of the new pile i, D_i^{End}, is only composed of the nonlinear displacement arising from its own loads, $D_i^{\mathrm{End,non}}$, and the elastic displacement induced by its adjacent existing pile, $D_{j,i}^{\mathrm{End,e}}$, i.e.

$$D_i^{\mathrm{End}} = D_i^{\mathrm{End,non}} + D_{j,i}^{\mathrm{End,e}} \tag{71}$$

The nonlinear displacement at the pile end can be calculated with Eq. (57) as

$$D_i^{\mathrm{End,non}} = \frac{Q(L)\left(c_{1,n} e^{r_n l(n-1)} + c_{2,n} e^{-r_n l(n-1)}\right)}{E_p A_p r_n \left(c_{1,n} e^{r_n L} - c_{2,n} e^{-r_n L}\right)} \tag{72}$$

The elastic displacement induced by adjacent existing displacement pile can be calculated from the Boussinesq's solution developed by Randolph and Wroth (1979a) in the following

$$D_{j,i}^{\mathrm{End,e}} = \frac{Q_{bj}\left(1 - v_{bj}\right)}{2 r_{j,i} G_{bj}} \tag{73}$$

Correspondingly, the elastic displacement induced by all the adjacent piles can be calculated as

$$D_{j,i}^{\mathrm{End,e}} = \sum_{j=1, j\neq i}^{n} \frac{Q_{bj}\left(1 - v_{bj}\right)}{2 r_{j,i} G_{bj}} \tag{74}$$

For the existing displacement piles in the pile group, the method for estimating their displacements is similar to that of new displacement piles stated above. To assess the load-displacement behavior of the pile group, a small displacement of pile end is first assumed and the midpoint displacement of pile segment is calculated. The difference between the end displacement and the midpoint displacement is checked. If it is smaller than a given tolerance, the load and displacement of next pile segment needs to be calculated. Otherwise, the end displacement of pile segment will be updated and the iterations will be conducted again until the difference is within the tolerance. After obtaining the load and displacement of the first pile segment, different displacements of pile end are assumed and the corresponding load and displacement of the first pile segment are calculated. Plotting the calculated loads and displacements of the first pile segment finally gives the load-settlement curve of the pile group.

7. Validation and discussion

7.1. In-situ test

The test site is located in Pudong New area, Shanghai, and used to be home to a glass factory that has been demolished but many displacement piles were left. Recently, a high-rise apartment, with 18 floors and a total height of about 60 m, was built on this site, with 22 of the existing displacement piles reused. The existing piles have been at the site for almost 30 years. Their length and diameter are 30 m and 0.5 m, respectively, and their measured elastic moduli are on the order of 36 GPa. To fully support the apartment, 74 new displacement piles with a length and diameter of 30 m and 0.4 m, respectively, were also installed into the clay strata to form the pile foundation. The measured elastic moduli of new piles are 30 GPa. Note that the existing piles are mainly located at the south of the building and the specific layout of new and existing piles is shown in Fig. 8. Eight monitoring points were arranged surrounding the building to correctly measure the vertical settlement of the building at the different stages of construction. The specific locations of these monitoring points can be also seen from Fig. 8.

Both the site investigation and the field boring log (see Fig. 9) show that the soil strata are chiefly composed of soft clay, clayey silt, mucky clay and silty clay from the top down. The soils are normally consolidated with an OCR in the order of 1.1. The secondary compression index of each clay stratum is about 0.00595. The height of each soil

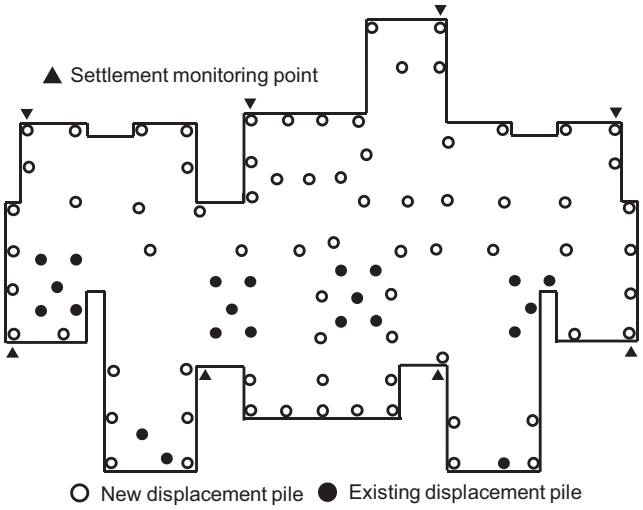

Fig. 8. Layout of displacement pile group for field test.

layer and other important soil parameters are summarized in Table 1. With the parameters of new and existing piles as well as each clay stratum, the proposed analytical framework is applied to predict the vertical settlement of the building after finishing the construction of each floor. In the calculation, the effective Poisson's ratio of clay is assumed to equal 0.3. A typical value of 0.8 is taken for the plastic volumetric strain ratio (Cao et al., 2001). The values of coefficient of earth pressure at rest, K_0, are estimated from the empirical formula proposed by Mayne and Kulhawy (1982) in the following

$$K_0 = \mathrm{OCR}^{\sin\varphi'}(1-\sin\varphi') \tag{75}$$

The raft of this building was designed as a rigid raft to eliminate the additional differential displacement due to the stiffness discrepancy among the new and existing piles. Hence, the raft displacement is identical to the displacement of the pile top. As a first approximation, the load shared by the raft, P_r, is estimated by Boussinesq's solution as

$$P_r = \frac{D_r E_r}{B\omega(1-v^2)} \tag{76}$$

where B is the raft width; ω is the shape factor of the raft and is often taken as 1 (Sheil and McCabe, 2016); $E_r = (E_{new}A_{new} + E_{ex}A_{ex} + E_sA_s)/A_r$ is the composite elastic modulus of the pile and the soil along the pile length; E_{new} and E_{ex} are the elastic moduli of new and existing piles, respectively; E_s is the elastic modulus of the soil beneath the raft; A_{new} and A_{ex} are the total areas of all new and existing piles, respectively; A_s is the total area of the soil beneath the raft; and A_r is the raft area. In the calculation, Eq. (76) together with the proposed method is applied to evaluate the displacement of pile groups.

Fig. 10 shows the comparison between the measured vertical settlement of the building and the predicted settlement of its pile foundation. Each data point corresponds to the settlement and load of the building after each floor was finished. When the whole building was finished, its total load was evaluated as about 275 MN. From the figure, it can be easily found that the predicted results exhibit a good agreement with the measured data, which demonstrates that the present analytical framework can be appropriately employed to predict the load-settlement behavior of pile groups composed of new and existing displacement piles. It can be also observed that the load transferred from the

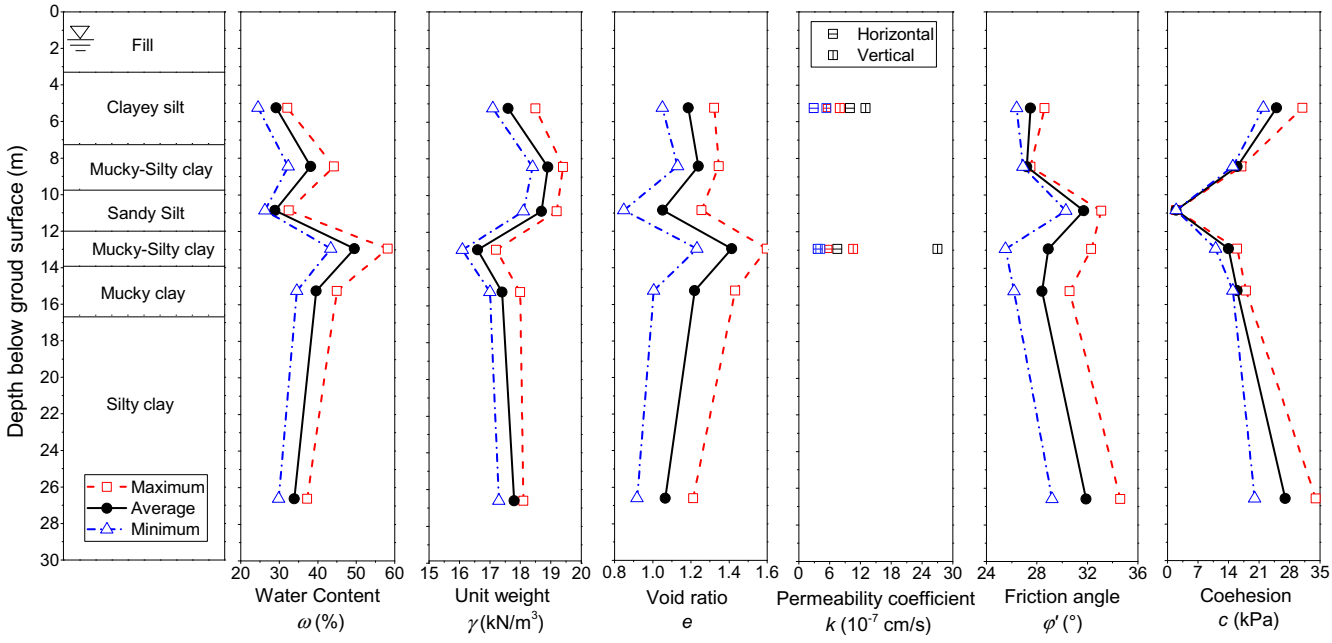

Fig. 9. Boring log at the field test site.

Table 1
Profile and basic properties of clay strata at test site.

Soil type	Thickness (m)	Effective unit weight (kN/m^3)	Friction angle (°)	Void ratio
Clay	3.3	8.9	31.7	1.052
Clayey silt	3.9	7.6	27.5	1.187
Mucky clay	9.4	7.4	28.4	1.219
Silty clay	20	7.8	31.9	1.065

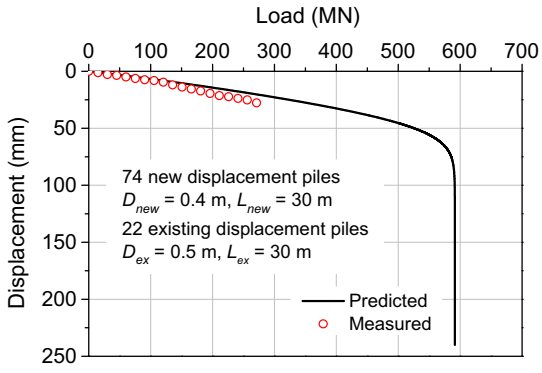

Fig. 10. Comparison between predicted and measured load-displacement behaviors of pile group consisting of new and existing displacement piles.

superstructure after the construction of building is far less than the ultimate load carrying capacity of the pile group, which indicates that the designed pile group can provide sufficient load carrying capacity to support the apartment.

7.2. Layout of new and existing displacement piles

To better investigate the load carrying behavior of pile groups consisting of new and existing displacement piles, it is of great requirement and significance to explore the different layouts of new and existing piles, since different layouts may lead to different load carrying behaviors of the pile group. Here, five different layouts of new and existing displacement piles are assumed: (a) all new piles; (b) only one existing pile located at the center; (c) four existing piles located at the edges; (d) four existing piles located at the corners; and (e) only one new pile located at the center. The specific layouts are shown in Fig. 11. A parameter, Ψ, which is referred to as the existing pile ratio, is defined as the ratio of the number of existing displacement piles to the number of total displacement piles to reflect the influence of the number of existing piles on the load carrying behavior of the pile group. The pile diameters and lengths of new and existing piles are the same, that is, 0.5 m and 30 m, respectively. The pile spacing is 1.5 m. The elastic moduli of new and existing piles are 30 GPa and 36 GPa, respectively. The soil parameters used in this analysis are the same as the parameters of the first-layer clay, which is tabulated in Table 1.

The stiffness of a single pile can be defined as the ratio of the load to the settlement of the pile head. Similarly, the

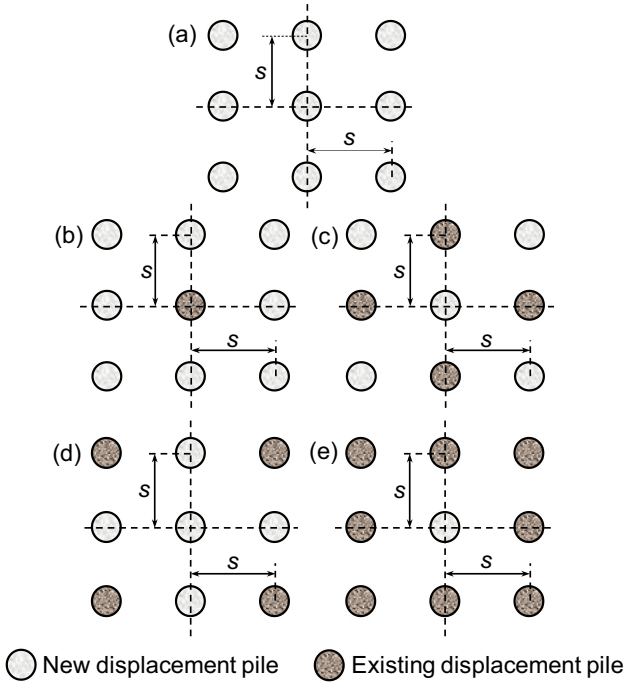

Fig. 11. Layout of pile group consisting of new and existing displacement piles: (a) all new piles; (b) existing pile at the center; (c) existing piles at the edges; (d) existing piles at the corners; (e) new pile at the center.

stiffness of a pile group can be defined as the load to the settlement of pile cap. In general, the stiffness of a pile group is much less than the sum of the stiffness of each single pile in the pile group, due to pile-pile interaction. Here, a parameter, referred to as the stiffness efficiency, is employed to directly reflect the influences of pile-pile interaction, which can be defined as the ratio of stiffness of pile group to the sum of stiffness of each single pile. Hence, the stiffness of the pile group consisting of new and existing piles can be defined as

$$\eta = \frac{K_{\mathrm{mix}}}{n(1-\Psi)K_{\mathrm{new}} + n\Psi K_{\mathrm{ex}}} \tag{77}$$

where n denotes the number of total piles; K_{new} represents the stiffness of new single pile; K_{ex} represents the stiffness of existing single pile; and K_{mix} denotes the stiffness of the pile group.

Fig. 12 shows the variation of stiffness efficiency of the pile group with five different layouts of new and existing piles. It can be found that the stiffness efficiency increases

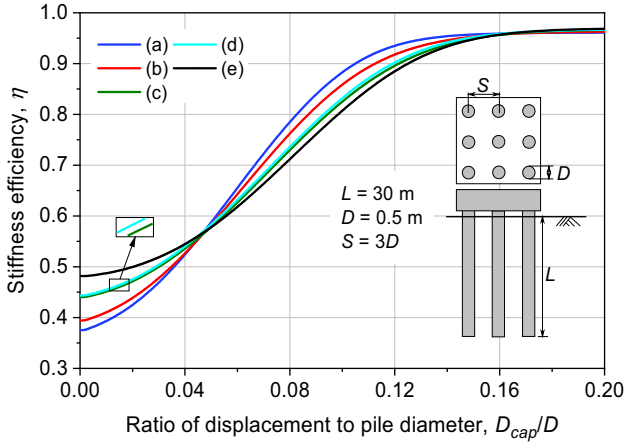

Fig. 12. Stiffness efficiency of pile groups consisting of new and existing displacement piles: (a) all new piles; (b) existing pile at the center; (c) existing piles at the edges; (d) existing piles at the corners; (e) new pile at the center.

with the increase in the settlement of the pile cap, but the initial stiffness efficiencies of pile groups with different existing pile ratios are different. This is because at the beginning of loading, the stiffness of the pile group depends on the stiffness of the individual piles and is significantly impacted by the pile-pile interaction. As the stiffness of the existing piles is stronger than the new piles, they provide more contributions to the overall stiffness of the pile group. Hence, according to the definition of the stiffness efficiency, the pile groups with different existing pile ratios show different initial stiffness efficiencies. In addition, it is interesting to note that when the ratio of the displacement to the pile diameter is below 0.04, the increase trends of stiffness efficiency differ from the increase trends when the ratio is above this value. The reason is that with development of the nonlinear behavior at the pile-soil interface, the stiffness of the existing pile reduces more significantly than the new pile and the portion of the stiffness provided by existing piles decreases. Simultaneously, the pile-pile interaction effect among individual piles reduces due to the nonlinear behavior of the individual pile. Therefore, the stiffness efficiencies increase from different values at the beginning to the same value as that when the ratio of the displacement to pile diameter is in the order of 0.04. After that, the stiffness of the existing pile still reduces more significantly than the new pile. Thus, the pile groups with different existing pile ratios again show different stiffness efficiencies until the individual pile reaches the ultimate state when the displacement of pile cap reaches about 0.16 times of the pile diameter. After reaching this displacement, the stiffness efficiency of all pile groups almost remains constant.

It can be also observed from Fig. 12 that at the beginning of loading, the stiffness efficiency of pile group with larger existing pile ratio is larger than that of pile group with smaller existing pile ratio. However, with the increase in the settlement of pile cap, the stiffness efficiency of pile group with smaller existing pile ratio will exceed the stiffness efficiency of pile group with larger existing pile ratio. The reason is that because of the effects of pile installation and soil aging, the undrained shear strength and shear modulus of clay around existing piles are much larger than those of clay around new piles. Therefore, the initial stiffness of existing pile is larger than that of new pile. However, due to the nonlinearity developed at the pile-soil interface, the tangential stiffness of existing pile decreases more rapidly with the increase in the settlement of pile cap than the new pile (Li et al. 2017a,b). In addition, it is worth noting that the pile groups with the same existing pile ratio (Layouts (c) and (d)) show almost the same stiffness efficiency, even though their layouts of new and existing piles are different.

Fig. 13 shows the load-displacement behavior of pile groups with five different layouts of new and existing displacement piles. It can be observed that both the stiffness and the ultimate load carrying capacity of the pile group increase with the increase in the existing pile ratio. This indicates that when the total number of piles in a pile group is determined, the load carrying capacity of the pile group will be generally larger if it has a larger existing pile ratio. Besides, in this analysis, when the pile groups have the same existing pile ratio (Layouts (c) and (d)), their stiffness and ultimate load carrying capacity are almost equal to each other, regardless of their different layouts. The reason is that although the overall load carrying behavior of the pile group is affected by the pile-pile interaction effects, the pile-pile interaction effects are almost the same for new and existing piles, as the soil among them behaves elastically. Compared with the pile-pile interaction effects, the stiffness of the individual pile has more significant effects on the overall load carrying behavior of the pile group when the nonlinear behavior of the individual pile is involved. Hence, if the existing pile ratio is the same, the overall stiffness and ultimate load carrying capacity of the pile groups are almost equal to each other. This work is by no means an exhaustive evaluation of pile groups with all possible pile numbers for different layouts. Hence, the

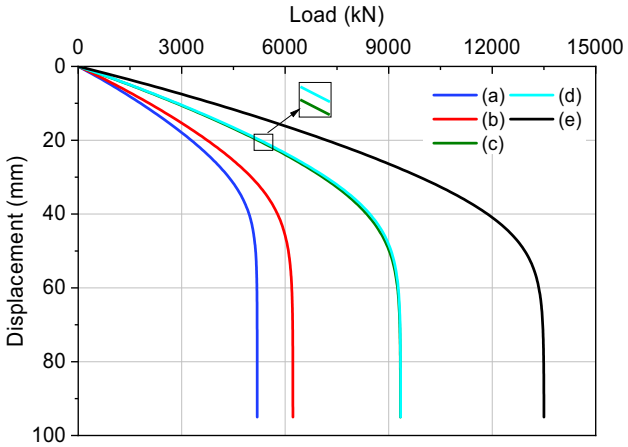

Fig. 13. Load-displacement behavior of pile groups consisting of new and existing displacement piles: (a) all new piles; (b) existing pile at the center; (c) existing piles at the edges; (d) existing piles at the corners; (e) new pile at the center.

typical 3 × 3 pile group with five different layouts of new and existing piles is investigated to demonstrate the important behavior for illustration purpose. Of course, this result may vary when the number of piles in the pile group is significantly higher.

8. Conclusions

This paper proposes an analytical framework to predict the load-displacement behavior of pile groups consisting of new and existing displacement piles. The load-transfer models for the new and existing piles are developed by appropriately considering the evolution of the strength and stiffness of the soil to model the nonlinear load-displacement behavior of the individual pile. The soil among the piles is assumed to behave elastically during loading and the pile-pile interaction effects are considered using the shear displacement method. The proposed analytical method not only incorporates the pile installation effects, subsequent consolidation and soil aging, but also properly considers the pile-pile interaction and the reinforcement effects of the adjacent pile. The validity of the proposed method is examined by predicting the settlement of a high-rise apartment during its construction. The predicted results agree well with the measured data, which demonstrates that the proposed framework can be applied to estimate the load carrying behavior of pile groups composed of new and existing piles. The major conclusions from this study are summarized as follows:

(a) Due to the effect of soil aging, the undrained shear strength and shear modulus of the clay around existing piles are much larger than those around new piles. Hence, existing piles show stiffer and stronger load carrying behavior than new piles.
(b) The pile group shows stronger stiffness and pile-pile interaction effects at the beginning of loading, but the stiffness reduces significantly with the nonlinear displacement developed at the pile-soil interface of individual piles.
(c) Compared with the pile-pile interaction effects, the stiffness of individual piles has more significant effects on the overall load carrying behavior of pile groups due to the nonlinear behavior of individual piles.
(d) The pile group with larger existing pile ratio shows stronger stiffness and higher load carrying capacity. However, for pile groups with the same existing pile ratio, the overall stiffness and ultimate load carrying capacity of pile groups almost equal each other, regardless of their different layouts of new and existing piles.

References

Abu-Farsakh, M., Rosti, F., Souri, A., 2015. Evaluating pile installation and subsequent thixotropic and consolidation effects on setup by numerical simulation for full-scale pile load tests. Can. Geotech. J. 52 (11), 1734–1746.

Augustesen, A.H., 2006. The effects of time on soil behaviour and pile capacity PhD Thesis. Aalborg University, Aalborg, Denmark.

Baligh, M.M., 1985. Strain path method. J Geotech. Eng. 111 (9), 1108–1136.

Bjerrum, L., 1967. Engineering geology of Norwegian normally-consolidated marine clays as related to settlements of buildings. Géotechnique 17 (2), 83–118.

Carter, J.P., Randolph, M.F., Wroth, C.P., 1979. Stress and pore pressure changes in clay during and after the expansion of a cylindrical cavity. Int. J. Numer. Anal. Meth. Geomech. 3 (4), 305–322.

Cao, L.F., Teh, C.I., Chang, M.F., 2001. Undrained cavity expansion in modified Cam clay: theoretical analysis. Géotechnique 51 (4), 323–334.

Garlanger, J.E., 1972. The consolidation of soils exhibiting creep under constant effective stress. Géotechnique 22 (1), 71–78.

Hazzar, L., Hussien, M.N., Karray, M., 2017. On the behaviour of pile groups under combined lateral and vertical loading. Ocean Eng. 131, 174–185.

Li, L., Li, J., Sun, D.A., 2016. Anisotropically elasto-plastic solution to undrained cylindrical cavity expansion in K_0-consolidated clay. Comput. Geotech. 73, 83–90.

Li, L., Li, J., Sun, D.A., Gong, W., 2017a. Analysis of time-dependent bearing capacity of a driven pile in clayey soils by total stress method. Int. J. Geomech. 17 (7). https://doi.org/10.1061/(ASCE)GM.1943-5622.0000860.

Li, L., Li, J., Sun, D.A., Gong, W., 2017b. An analytical approach for time-dependent load-settlement response of a jacked pile in clay strata. Can. Geotech. J. 54 (12), 1682–1692.

Matsuoka, H., Yao, Y., Sun, D., 1999. The Cam-clay models revised by the SMP criterion. Soils Found. 39 (1), 81–95.

Mayne, P.W., Kulhawy, F.H., 1982. K_0-OCR relationships in soil. J. Geotech. Eng. 108 (6), 851–872.

Randolph, M.F., 2003. Science and empiricism in pile foundation design. Géotechnique 53 (10), 847–876.

Randolph, M.F., Wroth, C.P., 1979a. An analysis of the vertical deformation of pile groups. Géotechnique 29 (4), 423–439.

Randolph, M.F., Wroth, C.P., 1979b. An analytical solution for the consolidation around a driven pile. Int. J. Numer. Anal. Meth. Geomech. 3 (3), 217–229.

Randolph, M.F., Wroth, C.P., 1981. Application of the failure state in undrained simple shear to the shaft capacity of driven piles. Géotechnique 31 (1), 143–157.

Roy, M., Blanchet, R., Tavenas, F., Rochelle, P.L., 1981. Behaviour of a sensitive clay during pile driving. Can. Geotech. J. 18 (1), 67–85.

Sheil, B.B., McCabe, B.A., Hunt, C.E., Pestana, J.M., 2015. A practical approach for the consideration of single pile and pile group installation effects in clay: numerical modelling. J. Geo-Eng. Sci. 2 (3), 1–21.

Sheil, B.B., McCabe, B.A., 2016. An analytical approach for the prediction of single pile and pile group behaviour in clay. Comput. Geotech. 75, 145–158.

Shen, W.Y., Chow, Y.K., Yong, K.Y., 1997. A variational approach for vertical deformation analysis of pile group. Int. J. Numer. Anal. Meth. Geomech. 21 (11), 741–752.

Skempton, A.W., 1959. Cast in-situ bored piles in London clay. Géotechnique 9 (4), 153–173.

Sun, D.A., Matsuoka, H., Yao, Y.P., Ishii, H., 2004. An anisotropic hardening elastoplastic model for clays and sands and its application to FE analysis. Comput. Geotech. 31 (1), 37–46.

Wang, Z., Xie, X., Wang, J., 2012. A new nonlinear method for vertical settlement prediction of a single pile and pile groups in layered soils. Comput. Geotech. 45, 118–126.

Wood, D.M., 1990. Soil Behaviour and Critical State Soil Mechanics. Cambridge University Press, Cambridge, U.K..

Zhang, Q.Q., Zhang, Z.M., 2012. A simplified nonlinear approach for single pile settlement analysis. Can. Geotech. J. 49 (11), 1256–1266.